Automated identification of discrepancies between nautical charts and survey soundings

Giuseppe Masetti [1,*], **Tyanne Faulkes** [2] **and Christos Kastrisios** [1]

[1] Center for Coastal and Ocean Mapping and NOAA-UNH Joint Hydrographic Center, University of New Hampshire, Durham, NH 03824, USA; gmasetti@ccom.unh.edu, ckastrisios@ccom.unh.edu

[2] NOAA National Ocean Service, Office of Coast Survey, Hydrographic Survey Division, Pacific Hydrographic Branch, Seattle, WA 98115-6349, USA; tyanne.faulkes@noaa.gov

* Correspondence: giuseppe.masetti@unh.edu, Tel.: +1-603-862-3452

Abstract: Timely and accurate identification of change detection for areas depicted on nautical charts constitutes a key task for marine cartographic agencies in supporting maritime safety. Such a task is usually achieved through manual or semi-automated processes, based on best practices developed over the years requiring a substantial level of human commitment (i.e., to visually compare the chart with the new collected data or to analyze the result of intermediate products). This work describes an algorithm that aims to largely automate the change identification process as well as to reduce its subjective component. Through the selective derivation of a set of depth points from a nautical chart, a triangulated irregular network is created to apply a preliminary tilted-triangle test to all the input survey soundings. Given the complexity of a modern nautical chart, a set of feature-specific, point-in-polygon tests are then performed. As output, the algorithm provides danger-to-navigation candidates, chart discrepancies, and a subset of features that requires human evaluation. The algorithm has been successfully tested with real-world electronic navigational charts and survey datasets. In parallel to the research development, a prototype application implementing the algorithm was created and made publicly available.

Keywords: nautical cartography; chart adequacy; change detection; triangulated irregular network; safety of navigation; ocean mapping

1. Introduction

The content of a nautical chart is derived from data sources that may greatly vary in quality and density [1,2]. It is also common to have, in a same nautical chart, parts based on modern high-resolution hydrographic surveys coexisting with areas not been resurveyed since eighteenth-century lead-line surveys [3]. At the same time, the recent evolution of shipping has both widened and increased the hydrographic needs, with new harbors and routes   established in areas that had never been surveyed [4]. And, on the other side, reasons of economic effectiveness cause merchant vessels to venture into approaches with less under keel clearance than before [3]. In addition, various natural events (e.g., hurricanes, high sedimentation rates) and human activities (e.g., dredging) may modify the condition of the premises and suddenly make obsolete parts or, in extreme cases, the entirety of a chart [5,6]. Thus, not only the quality of a nautical chart depends on the surveys upon which is derived but surveying for avoiding chart obsolescence represents a never-ending task.

After a survey, the newly collected datasets are evaluated for evidence of substantial changes against the latest relevant nautical charts. This operation must take into account the numerous transformations that a survey sounding has undergone from the moment that a sonar ping is emitted to its final representation on the chart, in particular when integrated on a statistically-based bathymetric surface and as the consequence of several possible cartographic adjustments (rounding and truncation, generalization, etc.) [7-10]. In addition, although ontologically distinct, disentangling inaccuracy and uncertainty adds complexity to the already challenging scenario [11]. Concurrently,

a general acceleration in the expected change rate of geospatial information during the past years pushes toward a much shorter updating cycle of nautical charts and, thus, a quick identification of discrepancies for a rapid dissemination of the required nautical information [2,3]. The identification of all the dangers to navigation (DtoNs) and navigationally significant features represents a challenge in complex surveys and significatively contributes to the total processing time of a new collected dataset [7]. The timely and accurate detection of the above represents a key task for cartographic agencies to fulfill their paramount objective to support the safety of navigation in the relevant waters.

Such a task is complicated by the intrinsic complex nature of a nautical chart as the result of a varying combination of human-driven considerations at the compilation time. Those considerations typically change from offshore to inshore, or along an open shoreline toward an intricate estuary [1]. Overall, the main criterion driving the chart compilation is the usefulness to the mariner in relation to the scale of the chart and the surrounding details [1]. Following such a criterion, a less significant feature is generally excluded (or reduced in emphasis) when its insertion may obscure other more important charted elements. In areas where detailed bathy-morphological information is required, a nautical chart provides a careful selection of trend-meaningful charted soundings and depth contours. This selection allows the chart user to interpret the morphology of the seabed by interpolating the provided bathymetric information in accordance with the shoal-biased source survey datasets. The nature of the interpolation is delegated to the end user, and it can be assumed that this mental process varies from a plain linear interpolation to a heavily biased interpolation toward the conservative side. The degree of bias is a combination of – both objective and subjective – contingent user considerations and, as such, difficult to be estimated. Together with the degree of interpolation bias, the likely existence of a few special cases related to the presence of feature types like marine farms, restricted areas, and other types of obstructions complicates the identification of discrepancies between nautical charts and the survey soundings [12].

The evaluation of current chart adequacy (as well as the rectification of possible deficiencies and shortcomings) represents a world-wide pressing need that poses a challenge to many national hydrographic offices [13,14]. Those offices must balance such a pressing need with the limited available resources and survey priorities that translate to the fact that decades may past until a new hydrographic survey can be conducted in a given area. In such an optic, it is becoming more and more obvious the requirement to evaluate the adequacy of the chart portfolio not only using newly collected bathymetric sonar bathymetry (BSB) but any possible source of geospatial information like automatic-identification system (AIS) data or alternative surveying means like synthetic aperture radar (SAR) shoreline extraction, satellite derived bathymetry (SDB) and airborne-lidar bathymetry (ALB)[6,14-20]. However, given the physically-limited penetration in water of SAR, SDB and ALB as well as the circular limitation in retrieving information from AIS data (i.e., vessels tend to avoid uncharted areas), BSB surveys – despite their high cost and logistic challenges – not only provide both highly accurate and dense measurements of the seafloor morphology, but also represent the only practical source of hydrographic information for large parts of the ocean [15].

The identification of nautical chart discrepancies in comparison to newly collected hydrographic survey datasets has received only limited attention in the scientific literature despite its importance for the safety of navigation and relevance in the evaluation of the adequacy of the current charts, as well as for coastal change analysis and coastal zone management [21-25]. In addition, many of the techniques developed for geospatial data analysis on land cannot be straightly applied to the nautical cartography realm, mainly because of the peculiar safety of navigation requirement [12,26-29]. Currently, the task to identify chart discrepancies against new BSB data sets is usually performed by the various cartographic agencies through manual or semi-automated processes, based on best practices developed over the years. However, these processes require a substantial level of human commitment that includes the visual comparison of the chart against the new data, the analysis of intermediate support products or, more commonly, a combination of the two.

This work describes an algorithm that aims to automate a large extent of the change detection process and to reduce its subjective human component. Through the selective derivation of a set of depth points from a nautical chart, a triangulated irregular network (TIN) is created to apply a

99   preliminary tilted-triangle test to all the input survey soundings. Given the complexity of a modern
100   nautical chart, a set of additional sounding-in-specific-feature tests are then performed. As output,
101   the algorithm provides DtoN candidates, chart discrepancies (the "deep" discrepancies may be
102   optionally identified), and a subset of features that requires human evaluation (if any). The algorithm
103   has been successfully tested with real-world Electronic Navigational Charts (ENCs) and survey
104   datasets. In parallel to the development of this work, an application implementing the algorithm was
105   created   and   made   publicly   available   in   the   HydrOffice   framework
106   (https://www.hydroffice.org/catools).

2. Materials and Methods

2.1. Electronic Navigational Charts

109   An ENC provides all the information for safe navigation in the form of a database – standardized
110   as to content, structure and format – issued on the authority of government authorized hydrographic
111   offices [30]. As such, it does not only contain information for safe navigation present in the
112   corresponding paper chart but can embed supplementary material present in other kinds of nautical
113   publications (e.g., sailing directions). The ENC content may be directly derived from original survey
114   material, but also from databased information, existing paper charts or a combination of them [31].
115   The International Hydrographic Organization (IHO) has created a standard vector format,
116   named S-57, for official ENCs (that is, produced by a government hydrographic office) that contain a
117   set of data layers for a range of hydrographic applications. However, an IHO S-57 ENC is mainly
118   used, in combination with positional information from navigation sensors and radar data, by an
119   Electronic Chart Display and Information System (ECDIS) to provide a graphical representation of a
120   marine area, including bathymetry and topography, and to assist the mariner in route planning and
121   monitoring by providing natural features, man-made structures, coastlines, and any other
122   information related to marine navigation [6,32]. To meet high standards of reliability and
123   performance, an extensive body of rules defines an ECDIS with the result that, under SOLAS Chapter
124   V regulations, an ECDIS loaded with official ENCs is currently the only alternative for the navigator
125   to the adequate and up-to-date paper charts [33].
126   As defined by the IHO standard, the S-57 data content consists of a set of features that may have
127   a spatial representation in the form of points, lines or polygons. Based on the ENC product
128   specifications, those features must be encoded using the chain-node topology (Figure 1) [32,34]. For
129   a S-57 ENC, the basic unit of geographic coverage is called "cell", normally a spherical rectangle
130   bordered by meridians and latitudes with actual data coverage of any shape [31]. Within the same
131   navigational purpose (e.g., coastal, approach) (Table 1), the cell data may not overlap with those of
132   the adjacent cells. The navigational purpose also drives the compilation scale and, thus, the features
133   contained in a cell.
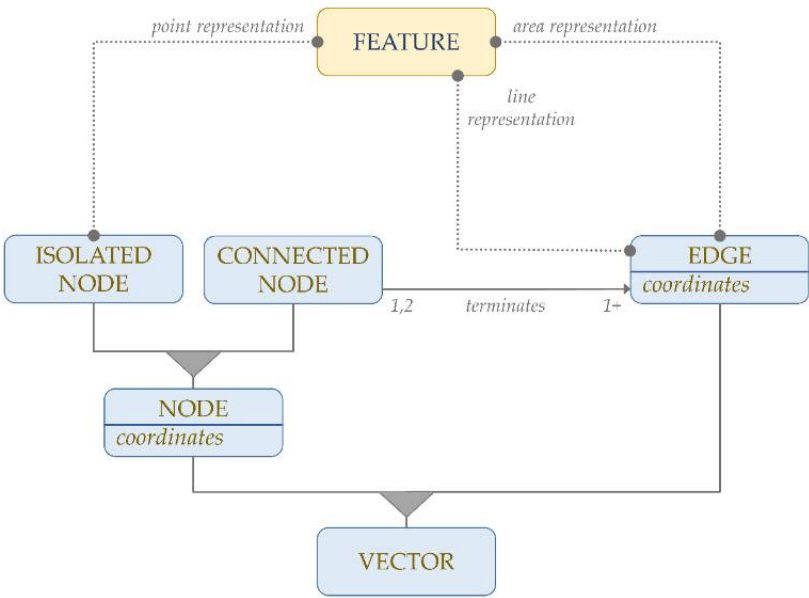
Figure 1. Graphical representation of the chain-node topologic model enforced by the S-57 ENC specifications. A geospatial feature may be represented as a point (by an isolated node), a line (using a series of edges and connected nodes), or an area (by a closing loop of edges starting and ending at a common connected node). Vector objects may be shared, but duplication of coincident linear geometry is prohibited [32].

Table 1. The ENC navigational purposes with range of compilation scales (and the standard radar scale within each range) suggested by the IHO S-65 publication [31].

ENC Navigational Purpose	Suggested Scale Range	Selectable Radar Range	Rounded Standard Scale
Overview	< 1:1,499,999	200 NM	1:3,000,000
		96 NM	1:1,500,000
General	1:350,000 – 1:1,499,999	48 NM	1:700,000
		24 NM	1:350,000
Coastal	1:90,000 – 1:349,999	12 NM	1:180,000
		6 NM	1:90,000
Approach	1:22,000 – 1:89,999	3 NM	1:45,000
		1.5 NM	1:22,000
Harbour	1:4,000 – 1:21,999	0.75 NM	1:12,000
		0.5 NM	1:8,000
Berthing	> 1:4,000	0.25 NM	1:4,000

2.2. Soundings from Bathymetric Sonar Surveys

In the hydrographic field, a sounding can be intended as a measured depth of water (i.e., a survey sounding) or as a bathymetric value represented on a nautical chart (i.e., a charted sounding) [30]. The algorithm described in this work digests both kinds of soundings, but with distinct uses. In fact, the survey soundings collected using bathymetric sonars – with multibeam sonars (MBES) currently playing a predominant role as acquisition devices – are analyzed as proxies for the bathy-morphology of the surveyed area [35], while the charted soundings represent one of the many feature types retrieved from the ENC to reconstruct the bathymetric model that the nautical cartographer wanted to communicate at the time of the ENC compilation (and, when present, after the application of all of the available ENC updates) .

153   The algorithm described in this work was developed to handle as input the following types of
154   survey soundings:
155   • "Pure survey soundings", intended as the point cloud measured by a bathymetric sonar after
156   having been properly integrated with ancillary sensors, cleaned by spurious measurements and
157   reduced to the chart datum.
158   • "Gridded survey soundings", represented by the nodes with valid depth values in a regularly-
159   spaced grid created using the pure survey soundings.
160   • "Selected gridded survey soundings", commonly generated during the cartographic processing
161   using algorithms that select the grid nodes that are more meaningful to depict the trend of the
162   underlining bathymetric model.
163   Assuming the correctness in the generation of the above three types of survey soundings (whose
164   evaluation is outside of the scope of the present work), the algorithm provides similar output results,
165   with the only relevant difference of the number of flagged features. The latter is justified by the
166   different number of survey soundings in input: the gridding and the selection processes commonly
167   reduce the amount of features input of one or more orders of magnitude.

168   *2.3. Bathymetric Model Reconstruction using a Triangulated Irregular Network (TIN)*

169   From a general point of view, a TIN consists of a network of irregular triangles generated by
170   connecting the nodes of a dataset in a way that guarantees the absence of intersecting triangle edges
171   and superposed triangle faces, but also that the union of all the triangles fills up the convex hull of
172   the triangulation (see Figure 2) [36]. For the aims of this work, we generate a TIN from a set of three-
173   dimensional nodes retrieved from the chart and then assume a linear variation of the bathymetric
174   model among those nodes.

175
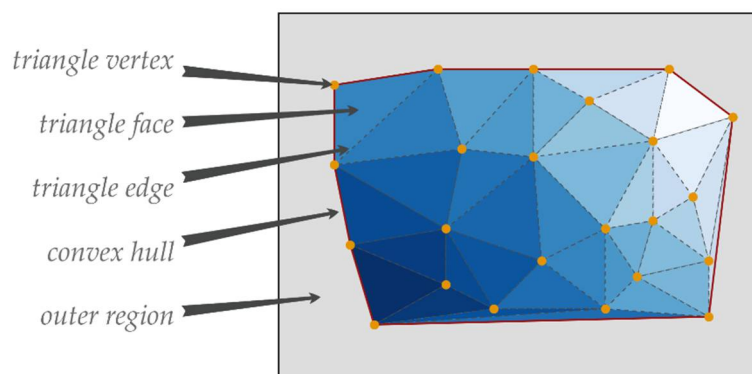
176   Figure 2. Example of a Triangulated Irregular Network (TIN) with the adopted nomenclature for the
177   various components.

178   The generated TIN is based on the Delaunay conforming triangulation [37] selected for the well-
179   known characteristic properties (e.g., being mathematically well defined, providing an unique output
180   for a given dataset independently from the data sequence) [38]. In the literature, several algorithms
181   implementing such a triangulation are available [39,40]. For the present work, we adopted the
182   practical convex hull algorithm that combines the two-dimensional Quickhull algorithm with the
183   general-dimension Beneath-Beyond algorithm, using the implementation provided by the open
184   source QHull code library [41].
185   For the bathymetric model reconstruction, the algorithm retrieves nodes from the following
186   ENC feature types (in parenthesis, the adopted S-57 acronym):
187   • Charted soundings (SOUNDG).
188   • Depth contour lines (DEPCNT) with a valid depth value attribute (VALDCO).
189   • Dredged area polygons (DRGARE) with a valid value for the minimum deptnh range attribute
190   (DRVAL1).
191   • All the point features with a valid value of sounding attribute (VALSOU).
192   • Natural (COALNE) and artificial (SLCONS) shorelines.

193  •  Depth area polygons (DEPARE) for the ENC cell boundaries only.

194  To avoid the creation of triangles crossing feature edges (and, thus, the corresponding
195 misrepresentation in the reconstructed bathymetric model), additional nodes are inserted along the
196 feature edges that are longer than the interpolation length (IL) of one centimeter ($k_{1cm} = 0.01m$) at
197 the ENC compilation scale (CS) (Figure 3):

$$IL = \frac{k_{1cm}}{CS}. \tag{1}$$

198  For example, with a CS value of 1:10,000, the IL obtained by applying (1) is 100 meters. Given
199 that the position of features in an ENC are provided in geographic coordinates referred to the World
200 Geodetic System 1984 Datum (WGS84), the metrical IL value is then converted to its corresponding
201 geographic value using the local latitude [31,32].

202  The algorithm retrieves the CS for (1) directly from the ENC, using the value stored in the
203 "Compilation Scale of Data" (S-57 label: CSCL) subfield in the "Data Set Parameter" (S-57 field tag:
204 DSPM) field structure [32]. By definition, such a value represents the compilation scale appropriate
205 to the greater part of the data in the cell [32]. The derivation of the interpolation factor, k, from the
206 ENC analysis (i.e., by looking at the distribution of the distance among the features) was attempted,
207 but it did not provide satisfying results, mainly because of the intrinsic variable-resolution nature of
208 a nautical chart. The one-centimeter interpolation value was then established heuristically as a trade-
209 off value between the requirement of avoiding the triangle-crossing-edge condition and the
210 performance cost paid for a larger point cloud to triangulate. The effectiveness of k_{1cm} has been
211 empirically tested using real-world ENCs, but more conservative values for k – or its derivation
212 from more advanced ENC analysis (e.g., locally estimating k rather than attempting to define a
213 single value for the full chart) – may be adopted.

214
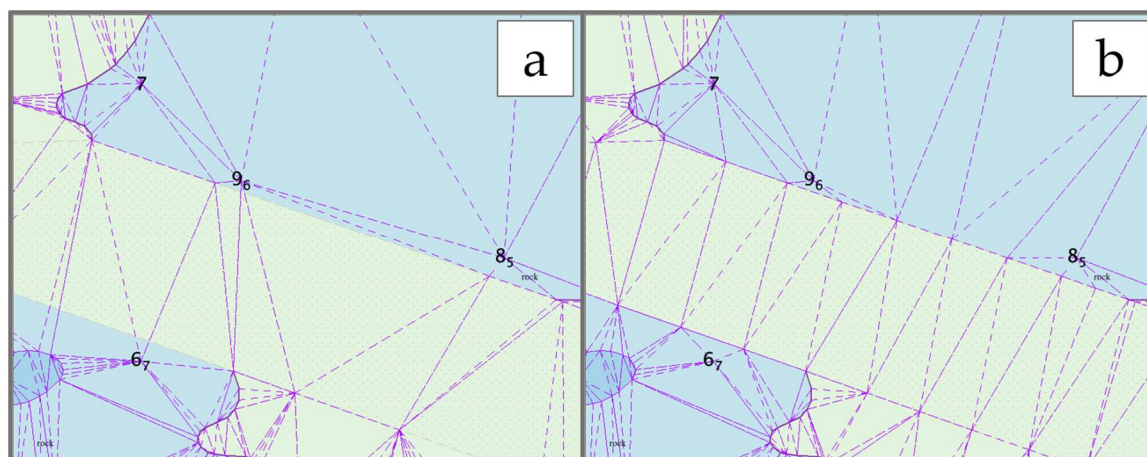
215  Figure 3. Pane (a) shows an example retrieved from an ENC where the long sides of a dredged-area
216  feature (visualized with a dotted pattern) trigger the creation of triangles (dashed magenta lines) that
217  overlap with the same feature edges. After the application of the proposed interpolation criterion, the
218  resulting triangulation shown in pane (b) does not present the overlap issue.

219  In addition to the described point densification, the reconstruction of a bathymetric model from
220 an ENC requires to associate a depth value to the nodes derived from the shoreline features, and that
221 such a value is referenced to the chart vertical datum like all the other depth nodes. Given that chart
222 producers may adopt different methods to identify the shoreline, the algorithm takes the depth value
223 for the shoreline as an input parameter. However, if not provided, the algorithm defaults to use the
224 shallowest depth value among all the valid depth values in the collected nodes.

225  The boundaries of the ENC bathymetry may be defined by the shoreline features and by the cell
226 data limits. In this latter case, based on the enforced chain-node topology, the algorithm retrieves the
227 nodes delimiting the point cloud by intersecting the depth area polygons along the cell boundaries
228 with the depth contour lines. At the resulting nodes is assigned the value of the minimum depth

229 range attribute (S-57 acronym: DRVAL1). In the rare cases where such a value is not populated in the
230 input ENC, the reconstruction of the bathymetric model along those edges cannot be performed and,
231 thus, the evaluation of any survey sounding present in these ambiguous areas is delegated to the
232 analyst.

233 *2.4. Application of the Tilted-Triangle Test*

234 Once the TIN has been generated, the input survey soundings are categorized after the
235 identification of the containing triangle. If a specific survey sounding is outside of all the TIN triangles
236 or is contained within a triangle with all the vertices having the same value (hereinafter referred to
237 as a "flat triangle"), the algorithm temporarily stages it for being re-examined in the step described
238 in the following section.
239 When an input sounding, S, is within a TIN triangle, the algorithm calculates the equation of
240 the tilted plane, $P(x, y, z)$, containing the three triangle vertices, U, V, W:

$$ax + by + cz + d = 0 \qquad (2)$$

241 where:

$$a = \begin{vmatrix} y_V - y_U & z_V - z_U \\ y_W - y_U & z_W - z_U \end{vmatrix},$$

$$b = \begin{vmatrix} z_V - z_U & x_V - x_U \\ z_W - z_U & x_W - x_U \end{vmatrix},$$

$$c = \begin{vmatrix} x_V - x_U & y_V - y_U \\ x_W - x_U & y_W - y_U \end{vmatrix}, \text{ and}$$

$$d = -(ax_U + by_U + cz_U).$$

242 The normal $\boldsymbol{n}$ for such a tilted plane can be calculated as:

$$\boldsymbol{n} = a\boldsymbol{i} + b\boldsymbol{j} + c\boldsymbol{k}. \qquad (5)$$

243 The vertical line containing the S point can be expressed in its parametric form, using S for the
244 position vector $\boldsymbol{t}$ and the line verticality for identifying the direction vector $\boldsymbol{v}$:

$$\boldsymbol{p} = \boldsymbol{t} + \lambda\boldsymbol{v} \qquad (3)$$

245 where the scalar λ varies to identify all the possible infinite point belonging to the vertical line.
246 After having identified both the vertical line passing for the sounding and the tilted plan, the
247 algorithm identifies the intersection point between the two geometrical entities by calculating λ
248 using [42]:

$$\lambda = \frac{-(\boldsymbol{n} \cdot \boldsymbol{t} + d)}{\boldsymbol{n} \cdot \boldsymbol{v}} \qquad (4)$$

249 The vertical distance, Δz_{SI}, is calculated as the difference between the depth dimensions between
250 the sounding, S, and its vertical interception point with the tilted plan, I:

$$\Delta z_{SI} = z_I - z_S. \qquad (6)$$

251 The algorithm uses the Δz_{SI} to evaluate whether flagging the soundings as DtoN candidates
252 (Figure 4) or potential chart discrepancies. The default logic of the applied thresholding (Table 2) is
253 derived from the NOAA Office of Coast Survey (OCS) Hydrographic Surveys Specifications and
254 Deliverables (HSSD) manual [43]. In deep waters, the DtoN concept does not apply to surface
255 navigation. However, based on the consideration that the presence of a very large discrepancy in
256 comparison to the charted water depth may represent an issue for specific marine operations (e.g.,
257 towing a side scan sonar), the algorithm reports – when using default parameters – potential DtoNs
258 for Δz_{SI} values larger than the ten percent of the water depth. However, since those values should
259 follow the specific policy (or other types of specific needs) of the adopting cartographic organization,
260 while the current ones are inspired by best practices in [43], the algorithm was made flexible to accept
261 customized threshold values as input parameters.

262
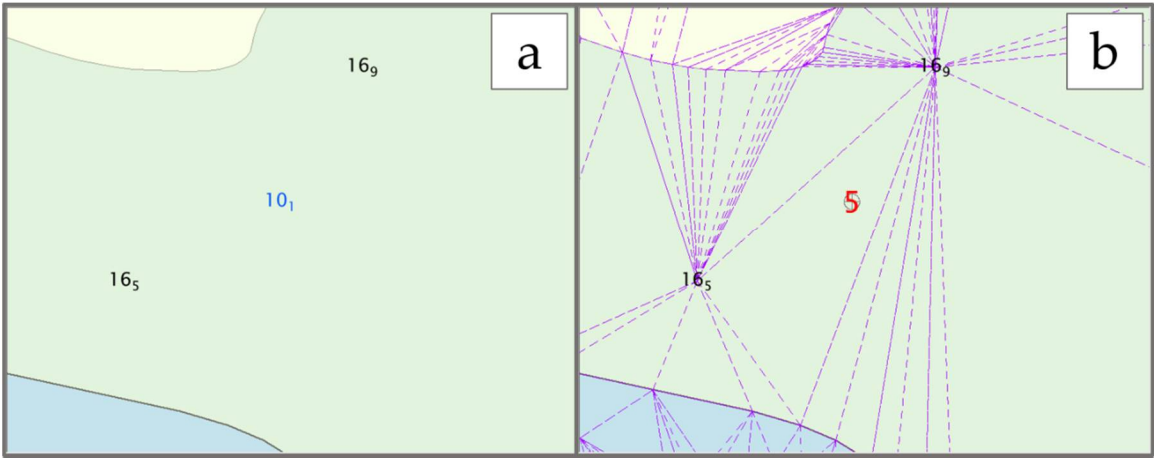
Figure 4. An example of DtoN detection. In the pane (a), a 10.1-meter survey sounding (in blue) is surrounded by two charted soundings (in black) and two depth contours of ten meters and twenty meters. The pane (b) shows the result of the triangulation (dashed lines in magenta) and a DtoN candidate (grey circle with a cross simple). This latter has a vertical distance of about five meters (red value overlaying the circle) from the underlying tilted triangle.

268

Table 2. Default threshold values adopted by the algorithm to identify the DtoN candidates and potential chart discrepancies. For depth values less than 20 meters, the adopted threshold follows best practices defined in the NOAA OCS HSSD manual [42]. Deeper waters have a much less compelling safety-of-navigation requirement; thus, the chosen percentages of water depth were selected after having considered the required IHO standard requirements for the original survey data. Adopting cartographic agencies should modify such values based on their adopted best practices.

Threshold type	z < 20 meters	z >= 20 meters
Danger to Navigation	1.0 meter	10.0 % of water depth
Chart Discrepancy	0.5 meter	5.0 % of water depth

275

Although large negative Δz_{SI} values ("deeps") do not represent a concern from a safety of navigation perspective, their presence provides evidence of chart inconsistencies. As such, the algorithm can be optionally set to identify those deeps, by simply applying a reversed thresholding logic in respect to the "shallow" chart discrepancies.

2.5. Application of the Sounding-in-Specific-Feature Tests

Due to the complexity of a modern nautical chart, the tilted-triangle test alone is not sufficient to properly evaluate all the possible feature configurations that can be depicted on an ENC. As such, the algorithm complements the described in paragraph 2.4 with a set of additional sounding-in-specific-feature tests.

From a geometrical point of view, the first common operation of such tests is to check whether a given sounding point is inside any of the polygons that belong to a specific feature type. Computationally, the detection of the presence of a point inside a polygon is most commonly done using the Ray Casting algorithm [44,45]. Among the several existing implementations available to assess topological relationship between geospatial objects, the algorithm adopted the vectorized binary predicates provided by the Shapely library [46].

A common use case of the point-in-polygon test is provided by the mentioned possible presence of a survey sounding within a flat TIN triangle. A flat triangle can be generated as the result of the triangulation in areas locally characterized by the presence of a linear feature – like a curved depth contour – not closely surrounded by other depth-defined features (Figure 5). In such a case, the

295 algorithm compares the given survey sounding against the validity depth range – when available –
296 of the underlying feature polygon (e.g., a depth area).

297
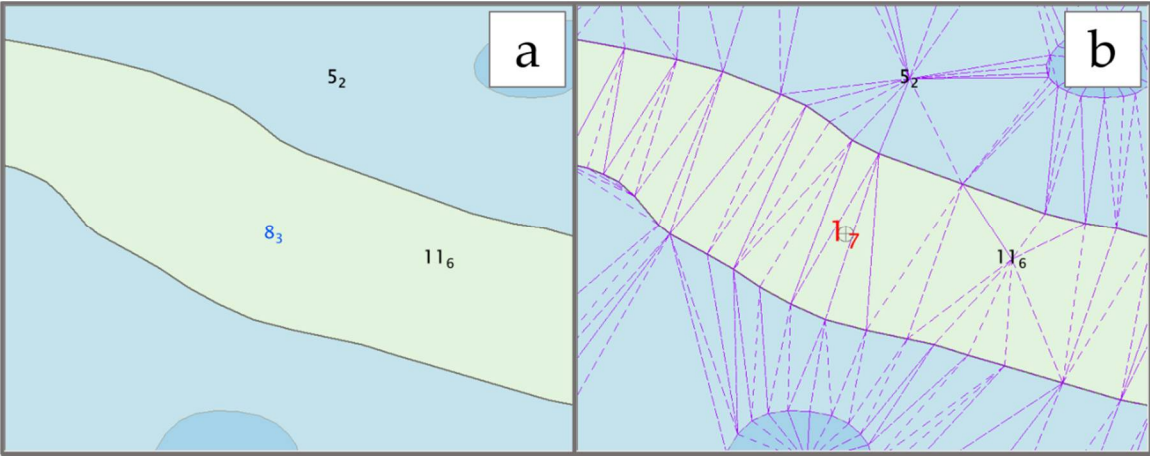
298 Figure 5. An example of presence of a survey sounding in a flat triangle. In the pane (a), an 8.3-meter
299 survey sounding (in blue) is surrounded by the nodes of a 10-meter depth contour that are closer than
300 the charted soundings (in black). As such, the survey sounding will be contained by a flat triangle
301 (that is, with three vertices having a 10-meter depth) shown in magenta in the pane (b). By adopting
302 the sounding-in-specific-feature test, the algorithm flagged the survey sounding as a potential
303 discrepancy (shown as grey circle with a depth difference of 1.7 meters in red) since it was detected
304 as contained by a depth area with a valid depth range between ten and twenty meters.

305 The S-57 ENC specifications prescribe that a cell must have the entire area with data covered,
306 without any overlap, by a restricted group of seven area feature types, called the "skin of the earth"
307 (Table 3) [32]. This characteristic of a S-57 ENC contributes to make the sounding-in-specific-feature
308 tests effective to reduce the number of staged untested features. Furthermore, if a survey sounding
309 is not contained in any of the skin of the earth polygons, it is outside of the ENC data coverage and
310 thus does not represent a chart discrepancy.

311 Table 3. The S-57 ENC area feature types, with the corresponding acronym, belonging to the restricted
312 "skin of the earth" group.

Feature Type	S-57 Acronym
Navigable depth areas	DEPARE
Dredged area	DRGARE
Floating dock	FLODOC
Permanently moored ship	HULKES
Land area	LNDARE
Pontoon	PONTON
Unsurveyed depth area	UNSARE

313
314
315 Figure 6 provides a flowchart outlining the main algorithmic steps, data inputs, user parameters,
316 and processing outputs. The plots provided in output should only be used for exploratory means. In
317 fact, once that the algorithm is successfully executed, the generated geospatial files should be
318 imported in the full-fledged GIS application of choice for results inspection and eventual application
319 of the required modifications to the ENC.
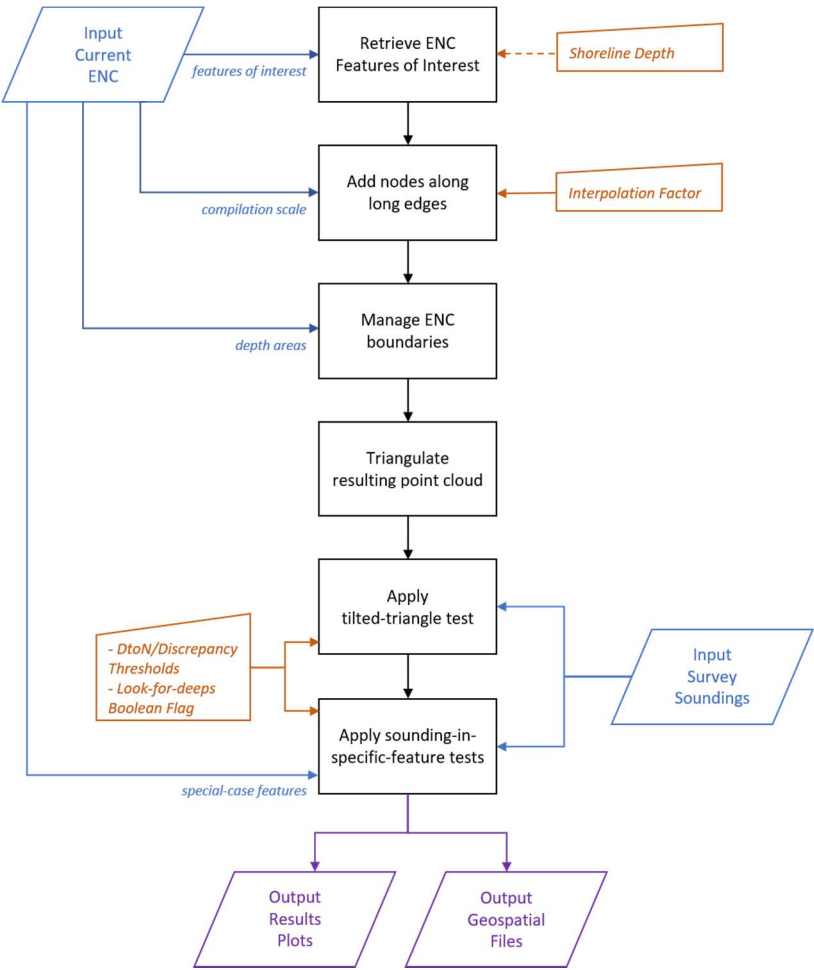
Figure 6. The flowchart shows, in black, the main steps of the proposed algorithm. The inputs are represented in blue, the user parameters in orange (with a dashed connector when optional), and the outputs in purple.

2.6. Library Implementation, Supporting Visualization, and Output Storage

A software library (current version: 1.0) that implements the algorithm has been developed and tested mostly using the Python language (version 3.6) [47]. For a few selected profiled bottlenecks, a superset of Python, called Cython (version 0.28) [48], was used to reduce the execution time by manually adding a few static type declarations. Using such declarations, Cython was then able to automatically convert Python code into optimized C code.

The library has been coupled with a multi-tab graphical user interface based on a Python port of the Qt framework [49]. The outcomes of the algorithm execution are visualized using the Matplotlib library [50]. ENC-derived depth values are colored by depth, while algorithm-flagged input survey soundings are colored by their discrepancy. If present, the subset of untested input soundings that require human evaluation are displayed with a magenta diamond. The default output is provided in S-57 format using internal code. For easy sorting and identification of discrepancies, the magnitude of the discrepancy against the chart is stored both as cartographic symbol features (S-57 acronym: $CSYMB) and soundings (i.e., storing the discrepancy value as the depth coordinate).

Optional output in the popular Shapefile and KML formats are generated using the Geospatial Data Abstraction Library (GDAL) package [51]. In this latter case, the TIN internally used by the algorithm is also generated for debugging aims. An implementation of the algorithm was made publicly available in the HydrOffice framework as a tab widget (Figure 7) freely accessible in the CA Tools application (https://www.hydroffice.org/catools).
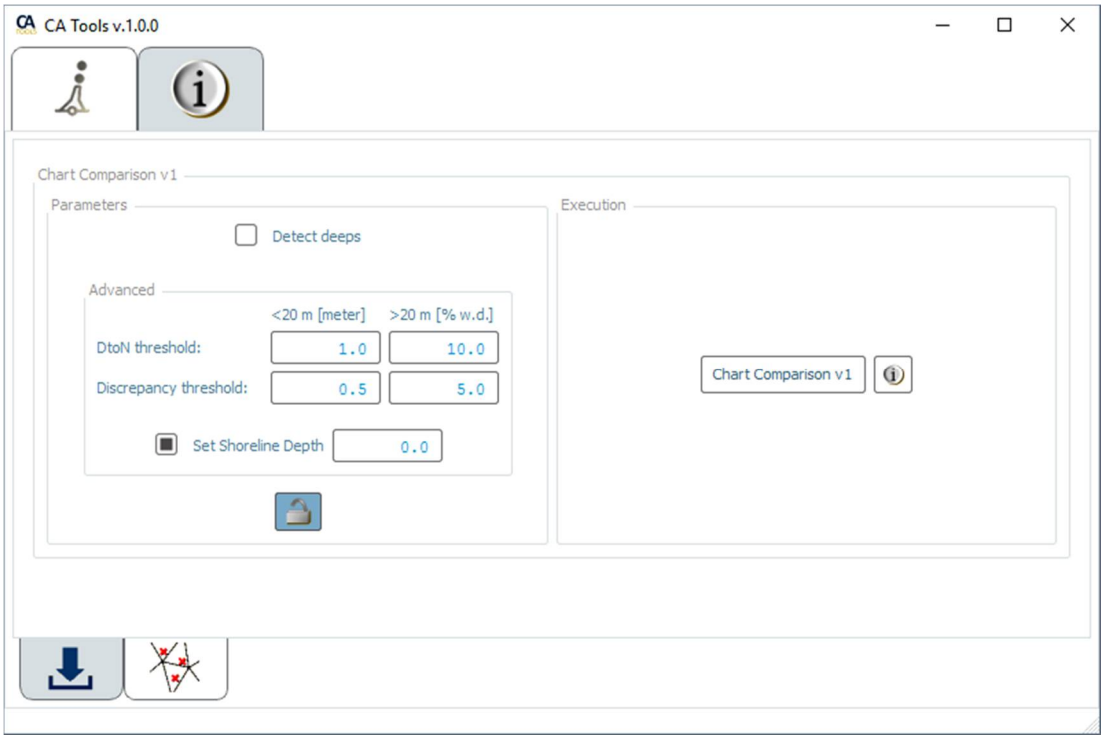
344   Figure 7. Screenshot of the tab widget present in the HydrOffice CA Tools application. The widget
345   exposes, on the left area, some of the algorithm parameters.

3. Results

347   At the best of our knowledge, the literature currently lacks algorithms specifically tailored to the
348   identification of discrepancies between nautical charts and survey soundings and, thus, with
349   outcomes directly comparable with the proposed algorithm. However, the algorithm results were
350   quantitatively compared, only for the DtoNs component, with the output of a tool named DtoN
351   Scanner (version 2) described in [25] and publicly available as part of the HydrOffice QC Tools
352   application (https://www.hydroffice.org/qctools/main). All the algorithm results were also validated
353   based on expert opinion.
354   During the initial development, *ad-hoc* input survey soundings have been generated with two
355   DtoNs and two chart discrepancies to be tested against a valid ENC. Using the described default
356   settings, the algorithm was able to identify both the DtoNs and the chart discrepancies Figure 8.
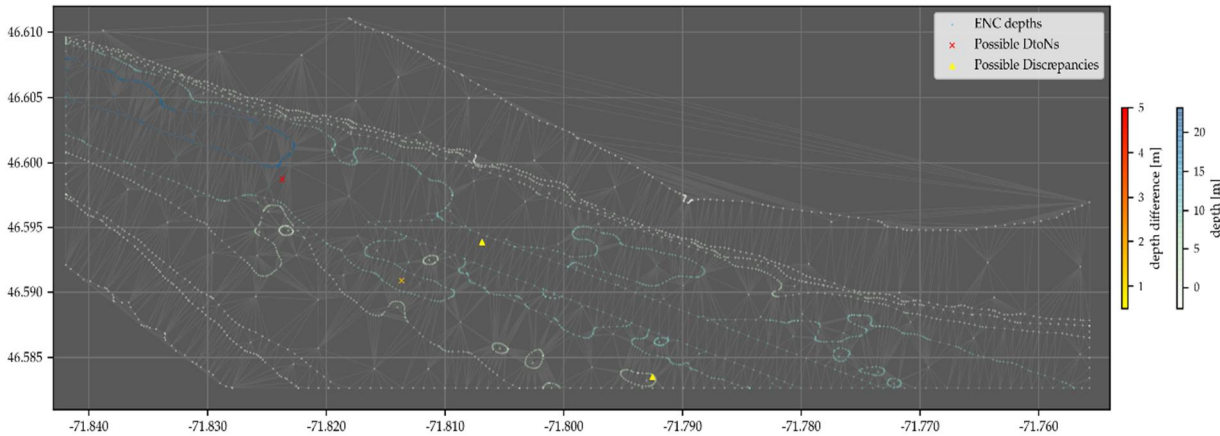
358   Figure 8. Algorithm results when applied to the *ad-hoc* input survey soundings. The possible DtoN
359   are presented using cross markers, while triangular markers are used for the possible discrepancies.
360   The nodes are represented as dots, with the connecting triangle edges in gray. Axes in geographical
361   WGS84 coordinates.

362   The algorithm has then been tested in several real-data scenarios using official ENCs and MBES-
363   based survey datasets. To keep this section concise, only two of those scenarios are here presented.
364   On one side, the analysis of the soundings from NOAA survey H12990 (see Figure 9) shows relatively
365   minor changes to the current ENCs. Conversely, the presence of large active glaciers in the area is
366   highlighted by the analysis of the NOAA H13701 dataset. Further details of the adopted inputs are
367   provided, for the surveys, in Table 4 and, for the ENCs, in Table 5.

368
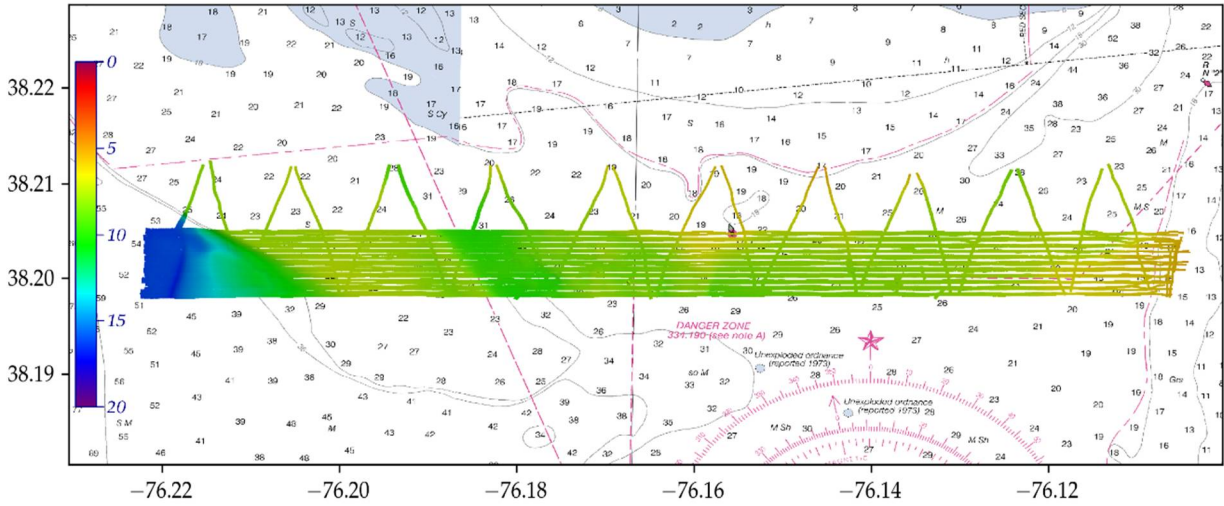
369   Figure 9. Bathymetric model generated using the data collected by the NOAA H12990 survey. The
370   NOAA raster nautical charts 12331 (Chesapeake Bay Tangier Sound Northern Part) and 12333
371   (Potomac River Chesapeake Bay to Piney Point) are shown in the background. Bathymetric values in
372   the color bar (in blues) are in meters and referred to the MLLW vertical datum. Axes in geographical
373   WGS84 coordinates.

374
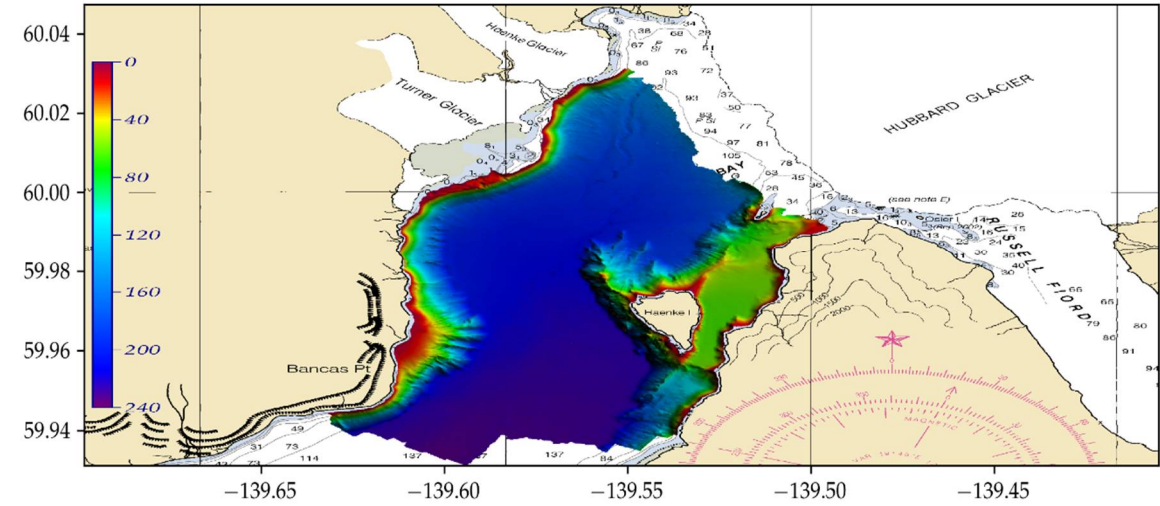
375   Figure 10. Bathymetric model generated using the data collected by the NOAA H13071 survey. The
376   NOAA raster nautical charts 16761 (Yakutat Bay) is shown in the background. Bathymetric values in
377   the color bar (in blue) are in meters and referred to the MLLW vertical datum. Axes in geographical
378   WGS84 coordinates.

379

380   Table 4. Information about the NOAA surveys presented as test datasets.

Survey	Location	Year	Scale	MBES
H12990	Chesapeake Bay (USA)	2017	1:10,000	Kongsberg EM 2040
H13071	Yakutat Bay (USA)	2017	1:40,000	Kongsberg EM 710, Kongsberg EM 2040

381   Table 5. Information about the NOAA ENCs used to test the algorithm.

Chart	Scale	Edition	Update Number	Issue Date
US5VA21M	1:40,000	21	0	2 May 2018
US5VA22M	1:40,000	28	2	5 June 2018
US4AK3XM	1:80,000	5	0	13 February 2018

382
383   The results of the analysis for the H12990 survey dataset are shown in Figure 11 and Figure 12.
384   These two figures represent the evaluation of the westernmost and easternmost parts, respectively of
385   the survey that insists in two different ENCs.

386
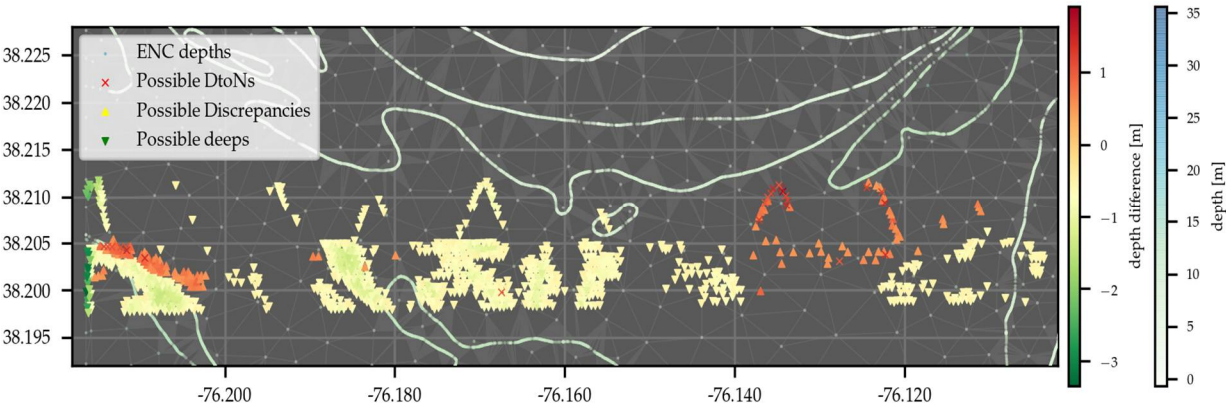
387   Figure 11. Algorithm results using the western part of the H12990 survey soundings compared to the
388   US5VA21M ENC. Axes in geographical WGS84 coordinates.

389
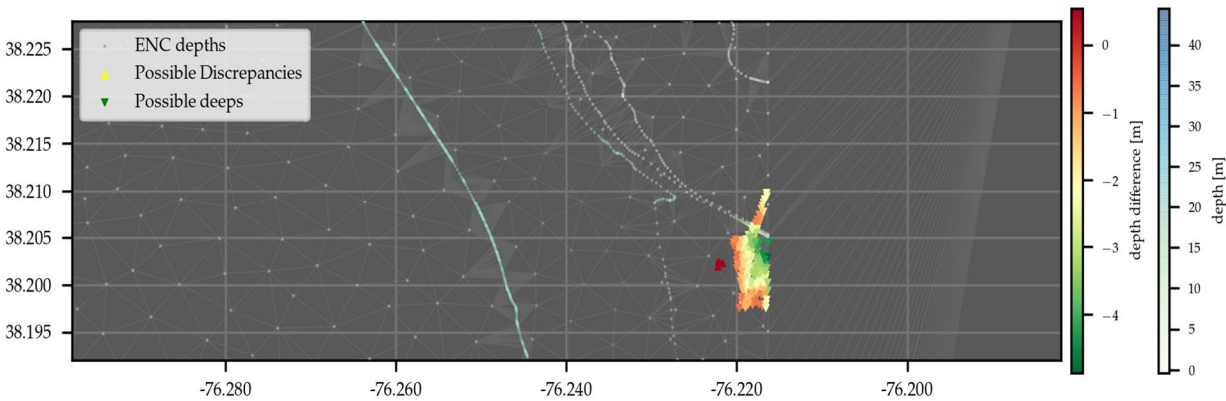
390   Figure 12. Algorithm results using the eastern part of the H12990 survey soundings compared to the
391   US5VA22M ENC. Axes in geographical WGS84 coordinates.

392   The results of the analysis for the H13701 survey dataset is shown in Figure 13.

393
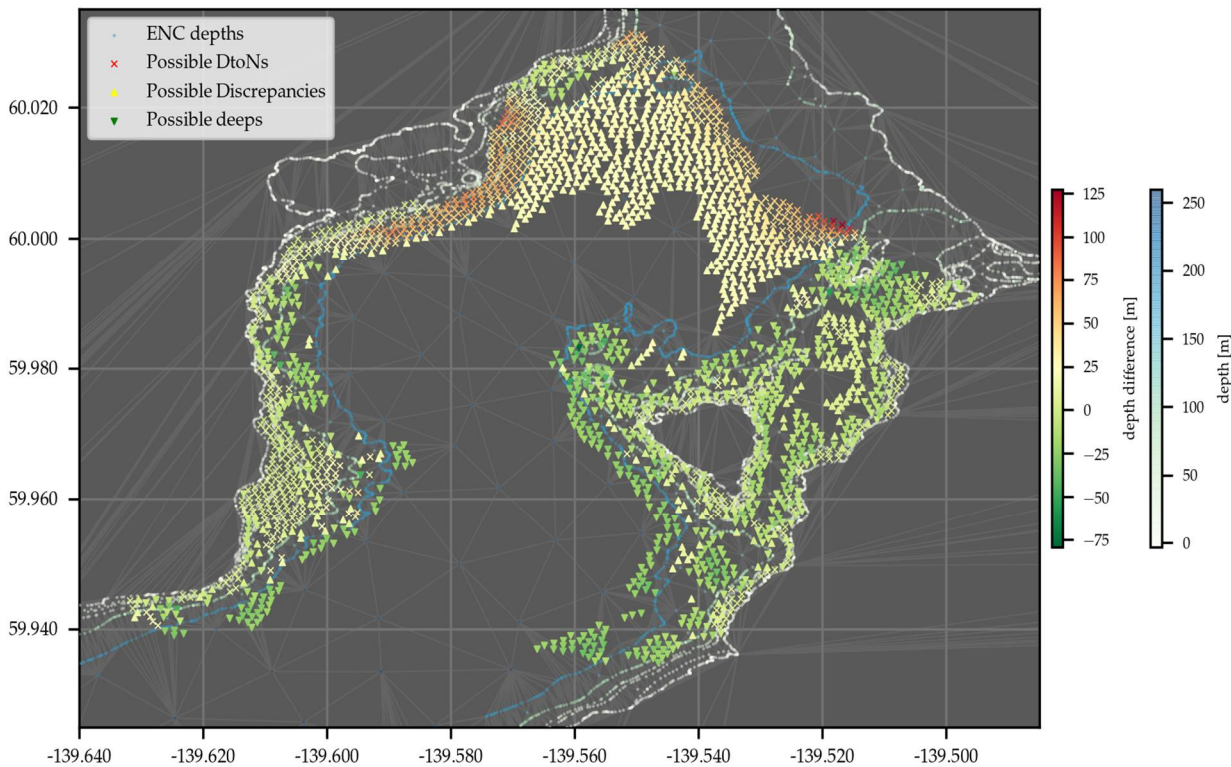
394   Figure 13. Algorithm results using the H13701 survey soundings compared to the US4AK3XM ENC.
395   Axes in geographical WGS84 coordinates.

396   The three applied analyses to the two presented surveys provide results that are consistent with
397   what reported by survey analysts – using their judgement to evaluate the context surrounding the
398   survey sounding, but with numeric criteria adherent to Table 2 – after a careful but time-consuming
399   evaluation of the same inputs (see Table 6, for DtoN candidates, and Table 7, for chart discrepancies).
400   The comparison with the expert opinion identified the presence of a few false positives (Table 7)
401   mainly localized close to the ENC boundaries. This is not surprising given the currently adopted
402   approach of using the minimum value in depth areas along the ENC boundaries for introducing
403   additional nodes. A possible future improvement to mitigate such an issue is the merge of point
404   clouds retrieved from adjacent ENCs – at the same navigational purpose – before performing the
405   "Triangulate resulting point cloud" step (Figure 6).
406   For the DtoNs candidates, the proposed algorithm performed better than the DtoN Scanner in
407   terms of both false negatives and false positives. The better performance can be reconducted to the
408   adoption of more capable tests (the DtoN Scanner only uses a "flat" triangle test with the shallowest
409   depth of each triangle vertices) and the additional techniques adopted during the construction of the
410   point cloud from the ENC (e.g., the long-edge interpolation, the adoption of a proper shoreline depth
411   value, the retrieval of the ENC boundaries).

412   Table 6. Results for DtoN candidates using the proposed algorithm and the DtoN Scanner [25]. The
413   Expert Opinion column provides the total number of DtoNs used to identify the false negatives (FN)
414   and the false positives (FP) for the two sets of automated outputs.

Input Pair	Expert Opinion	Proposed Algorithm			DtoN Scanner		
		Total	*FN*	*FP*	Total	*FN*	*FP*
Ad-hoc data pair	**2**	**2**	*0*	*0*	**1**	*1*	*0*
H12990, US5VA21M	**25**	25	*0*	*0*	23	*7*	*5*
H12990, US5VA22M	**0**	0	*0*	*0*	1	*0*	*1*
H13701, US4AK3XM	**713**	713	*0*	*0*	674	*51*	*12*

415

416   Table 7. Results for chart discrepancies using the proposed algorithm. The Expert Opinion column
417   provides the total number of chart discrepancies used to identify the false negatives (FN) and the false
418   positives (FP) for the automated output.

Input Pair	Expert Opinion	Proposed Algorithm		
		Total	*FN*	*FP*
Ad-hoc data pair	**2**	**2**	*0*	*0*
H12990, US5VA21M	**107**	**110**	*0*	*3*
H12990, US5VA22M	**2**	**3**	*0*	*1*
H13701, US4AK3XM	**779**	**784**	*0*	*5*

419

4. Discussion

421   Although the algorithm has been successfully tested with several pairs of real-world ENCs and
422   survey datasets, more tests are required to identify possible shortcomings and corner cases absent in
423   the analyzed scenarios. However, the handling of eventual issues will likely happen by extending the
424   described two-step approach and, thus, preserve the general validity of the algorithm proposed in
425   this work.
426   Although popular, the IHO S-57 ENC format is not the only available format to store the
427   geospatial vector information of a nautical chart for use with an ECDIS (e.g., the National Geospatial
428   Agency's Digital Nautical Chart format, the coming IHO S-101 standard) [33,52]. Although this work
429   is based only on ENC data in the IHO S-57 format, the extension to other ENC formats should be
430   straightforward.
431   The survey soundings are ultimately limited by the quality of the original observations used to
432   sample the seafloor [53]. This consideration acquires increasing relevance when the dimensions of
433   the measured chart discrepancies approaches the limits – that should be experimentally evaluated or
434   retrieved by the specifications declared by the manufacturer – of the sonar system used for the survey
435   [54]. The sonar detection uncertainty represents just one potential source of artifacts with a variety of
436   other potential environmental, integration and datum reduction issues that can badly affect the final
437   survey soundings [35,55]. When this happens, bathymetric artifacts generated by the acoustic
438   imaging geometry may be mistaken as chart discrepancies. Among other institutions, the
439   International Hydrographic Organization has developed rules and best practices for the execution of
440   a hydrographic survey that fulfills minimum quality requirements for charting aims [56,57].
441   However, the execution of a hydrographic survey is not always targeted at the production of nautical
442   charts. New hydrographic data are collected for a variety of reasons that spans from scientific
443   research to military applications and marine constructions [58]. Given the high cost of data collection
444   at sea, the national hydrographic offices usually attempt to use those surveys, when made them
445   available, for charting purposes. As such, a buffer representing a lower limit of what is considered a
446   chart discrepancy should also consider an estimation of the soundings quality based on the specific
447   survey being analyzed.
448   A preliminary step in the application of the algorithm consists in the retrieval of the information
449   content present in the input ENC. Ideally, such a content should be used to reconstruct a continuous
450   bathymetric model of the ENC's underwater area that matches – as close as possible – the intent of
451   the chart makers and the expectations of the chart readers. In practice, it is unlikely that, based on
452   different precautionary principles and contingent valuations, two random navigators would draw a
453   perfectly overlapping intermediate contour on a given ENC area. Given the complexity and inherent
454   subjectivity involved in the bathymetric reconstruction, we opted for a simplified, still reasonable
455   solution for the task by generating a TIN from the set of three-dimensional nodes retrieved from the
456   chart and then assuming a linear variation of the model among those nodes.
457   In alternative to the use of the Delaunay conforming triangulation, future works may explore
458   the creation of the TIN based on a constrained Delaunay triangulation [59,60], since this technique
459   makes possible to explicitly define edges ("breaklines") that are not modified by the triangulator
460   (thus removing the currently required addition of interpolated nodes along long edges). However,

461 the adopted point densification for long feature edges provides a controlled mean to introduce nodes
462 in the triangulation. Thus, we will likely also explore the adoption of a hybrid solution.
463   The conversion by interpolation of a TIN into a regular grid to perform discrepancy analysis
464 represents a quite popular operation. However, although the several intrinsic advantages related to
465 deal with grid data (e.g., higher processing and development speed) [36], we decided to not take such
466 a direction because of the intrinsic variable-resolution nature of an ENC that makes difficult to
467 identify the best fixed resolution at which to grid the TIN. Regarding the possible creation of a
468 variable-resolution grid, despite the recent development and successful application of this type of
469 gridding algorithms to MBES data [61], a robust estimation of the local resolution based on a ENC-
470 derived data would have represented a challenge, and it is an open research question.
471   At the best of our knowledge, this work represents the first appearance in literature of a
472 proposed algorithm for identifying discrepancies between nautical charts and survey soundings.
473 Thus, there is a lack of research efforts that the results of this work can be directly compared with,
474 with the notable exception of the DtoN Scanner [25]. However, the described tilted-triangle test may
475 be seen as an evolution of a well-known best practice in nautical cartography for the representation
476 of depth during chart compilation [21]. Such a practice, known as the "triangular method of selection"
477 [62], is commonly used to drive the selection of the charted soundings, and it is based on the following
478 two tests:

- Triangle test. Within a triangle of charted soundings, no survey sounding is present which is less than the shallowest depth values defining the corners of the triangle.
- Edge test. Between two adjacent charted soundings, no survey sounding exists shallower than the lesser of the two charted soundings.

483   The application of those tests presents some well-known scale- and data density-dependent
484 issues (e.g., which spatial buffer to apply for the edge test? What is the significance of the triangle test
485 with narrow elongated triangles?) that the tilted-triangle test potentially overcomes.

5. Conclusions

487   The present work provides evidence that, with respect to chart adequacy assessment, the
488 adoption of the described two-step algorithm brings several improvements (e.g., less subjectivity and
489 time of execution) in comparison to the current commonly-adopted practices.
490   Future works will focus on exploring techniques to better reconstruct the bathymetric model
491 from ENCs (i.e., attempting to better capture the cartographer and the mariner interpretations of the
492 charted bathymetry) and evaluating the adaptation of the algorithm to chart compilation aims as a
493 replacement of the triangle test and the edge test.

Author Contributions: Methodology and data curation: G.M., T.F. and C.K.; software and visualization: G.M.; formal analysis: G.M. and C.K.; validation, investigation, and resources: T.F.; writing—original draft preparation: G.M.; writing—review and editing: T.F. and C.K.

Funding: This research was partially funded by the NOAA grant NA15NOS4000200.

Acknowledgments: Authors would like to thank the NOAA National Ocean Service (NOS) Office of Coast Survey (OCS) and the Canadian Hydrographic Service (CHS) for the datasets, Mathieu Rondeau (CHS Waterways Surveys Unit), Claude Tremblay (CHS Maurice Lamontagne Institute), and Peter Holmberg (NOAA NOS Office of Coast Survey, Pacific Hydrographic Branch) for their support. Authors are also grateful to the anonymous reviewers whose comments helped to improve the paper.

Conflicts of Interest: The authors declare no conflict of interest.

References

1.   Russom, D.; Halliwell, H. Some Basic Principles in the Complication of Nautical Charts. *The International Hydrographic Review* **1978**, *55*.

508　2.　Mayer, L.; Jakobsson, M.; Allen, G.; Dorschel, B.; Falconer, R.; Ferrini, V.; Lamarche, G.; Snaith, H.;
509　　　Weatherall, P. The Nippon Foundation—GEBCO Seabed 2030 Project: The Quest to See the World's Oceans
510　　　Completely Mapped by 2030. *Geosciences* **2018**, *8*, 63, https://doi.org/10.3390/geosciences8020063.

511　3.　Pasquay, J.-N. Safety of modern shipping and requirements in hydrographic surveying and nautical
512　　　charting. *The International Hydrographic Review* **1986**, *63*.

513　4.　Buixadé Farré, A.; Stephenson, S.R.; Chen, L.; Czub, M.; Dai, Y.; Demchev, D.; Efimov, Y.; Graczyk, P.;
514　　　Grythe, H.; Keil, K., *et al.* Commercial Arctic shipping through the Northeast Passage: routes, resources,
515　　　governance, technology, and infrastructure. *Polar Geography* **2014**, *37*, 298-324,
516　　　https://doi.org/10.1080/1088937X.2014.965769.

517　5.　Masetti, G.; Calder, B. *A Bayesian marine debris detector using existing hydrographic data products*, OCEANS
518　　　2015 - Genova, 18-21 May 2015, 2015; pp 1-10, https://doi.org/10.1109/OCEANS-Genova.2015.7271584.

519　6.　Roh, J.Y.; Shin, M.S.; Suh, Y.C.; Yang, I.T.; Lee, D.H. Evaluation of Nautical Chart Adequacy in the Coastal
520　　　Area around Incheon Bay using Satellite Imagery with AIS Data. *Journal of Coastal Research* **2017**, 319-323,
521　　　https://doi.org/10.2112/SI79-065.1.

522　7.　Moegling, C.; Holmberg, P. *Journey of a Sounding: Application of NOAA Soundings and Features to Navigation*
523　　　*Products*, U.S. Hydro Conference, New Orleans, LA, USA, 2013; New Orleans, LA, USA, p 17.

524　8.　Calder, B.; Mayer, L. Automatic Processing of High-Rate, High-Density Multibeam Echosounder Data.
525　　　*Geochemistry Geophysics And Geosystems* **2003**, *4*, https://doi.org/10.1029/2002GC000486.

526　9.　Shea, K.S.; McMaster, R.B. *Cartographic generalization in a digital environment: When and how to generalize*,
527　　　Proceedings Auto-Carto, 1989; pp 56-67.

528　10.　Gökgöz, T.; Sen, A.; Memduhoglu, A.; Hacar, M. A New Algorithm for Cartographic Simplification of
529　　　Streams and Lakes Using Deviation Angles and Error Bands. *ISPRS International Journal of Geo-Information*
530　　　**2015**, *4*, 2185, http://dx.doi.org/10.3390/ijgi4042185.

531　11.　Tucci, M.; Giordano, A. Positional accuracy, positional uncertainty, and feature change detection in
532　　　historical maps: Results of an experiment. *Computers, Environment and Urban Systems* **2011**, *35*, 452-463,
533　　　https://doi.org/10.1016/j.compenvurbsys.2011.05.004.

534　12.　James, L.A.; Hodgson, M.E.; Ghoshal, S.; Latiolais, M.M. Geomorphic change detection using historic maps
535　　　and DEM differencing: The temporal dimension of geospatial analysis. *Geomorphology* **2012**, *137*, 181-198,
536　　　https://doi.org/10.1016/j.geomorph.2010.10.039.

537　13.　IHO. *C-55: Status of Hydrographic Surveying and Charting Worldwide*; Edition 31 July 2018; International
538　　　Hydrographic Organization: Monaco, 2018; p 528.

539　14.　Klemm, A.; Pe'eri, S.; Freire, R.; Nyberg, J.; Smith, S.M. *Nautical Chart Adequacy Evaluation Using Publicly-*
540　　　*Available Data*, U.S. Hydro Conference, National Harbor, MA, USA, 2015; National Harbor, MA, USA, p 6.

541　15.　Chénier, R.; Faucher, M.-A.; Ahola, R. Satellite-Derived Bathymetry for Improving Canadian
542　　　Hydrographic Service Charts. *ISPRS International Journal of Geo-Information* **2018**, *7*, 306,
543　　　https://doi.org/10.3390/ijgi7080306.

544　16.　Lyzenga, D.R. Shallow-water bathymetry using combined lidar and passive multispectral scanner data.
545　　　*International Journal of Remote Sensing* **1985**, *6*, 115-125, https://doi.org/10.1080/01431168508948428.

546　17.　Stumpf, R.P.; Holderied, K.; Sinclair, M. Determination of water depth with high-resolution satellite
547　　　imagery over variable bottom types. *Limnology and Oceanography* **2003**, *48*, 547-556,
548　　　https://doi.org/10.4319/lo.2003.48.1_part_2.0547.

549　18.　Su, H.; Liu, H.; Heyman, W.D. Automated Derivation of Bathymetric Information from Multi-Spectral
550　　　Satellite Imagery Using a Non-Linear Inversion Model. *Marine Geodesy* **2008**, *31*, 281-298,
551　　　https://doi.org/10.1080/01490410802466652.

552　19.　Pe'eri, S.; Parrish, C.; Azuike, C.; Alexander, L.; Armstrong, A. Satellite Remote Sensing as a
553　　　Reconnaissance Tool for Assessing Nautical Chart Adequacy and Completeness. *Marine Geodesy* **2014**, *37*,
554　　　293-314, https://doi.org/10.1080/01490419.2014.902880.

555　20.　Pe'eri, S.; Madore, B.; Nyberg, J.; Snyder, L.; Parrish, C.; Smith, S. Identifying Bathymetric Differences over
556　　　Alaska's North Slope using a Satellite-derived Bathymetry Multi-temporal Approach. *Journal of Coastal*
557　　　*Research* **2016**, 56-63, https://doi.org/10.2112/SI76-006.

558　21.　Wilson, M.; Masetti, G.; Calder, B.R. Automated Tools to Improve the Ping-to-Chart Workflow.
559　　　*International Hydrographic Review* **2017**, *17*, 21-30.

560　22.　Azuike, C.; Pe'eri, S.; Alexander, L.; Parrish, C.; Armstrong, A. *Development of a Geo-spatial Analysis*
561　　　*Methodology for Assessing the Adequacy of Hydrographic Surveying and Nautical Charts*, Canadian
562　　　Hydrographic Conference, Niagara Falls, Ontario, Canada, May 15 - May 17, 2012, 2012; Niagara Falls,
563　　　Ontario, Canada.

564　23.　Moitoret, V.; Johnson, N.E. Automation of Hydrographic Source Data. *The International Hydrographic Review*
565　　　**1967**, *45*.

566 24. Furuya, H. Automating the Marine Chart Production Processes. *Cartographica: The International Journal for*
567   *Geographic Information and Geovisualization* **1973**, *10*, 23-36, https://doi.org/10.3138/6716-9222-4534-3440.
568 25. Wilson, M.; Masetti, G.; Calder, B. *NOAA QC Tools: Origin, Development, and Future*, Canadian
569   Hydrographic Conference, Halifax, Nova Scotia, Canada, 2016; Halifax, Nova Scotia, Canada.
570 26. Qi, H.B.; Li, Z.L.; Chen, J. Automated change detection for updating settlements at smaller-scale maps from
571   updated   larger-scale   maps.   *Journal   of   Spatial   Science*   **2010**,   *55*,   133-146,
572   https://doi.org/10.1080/14498596.2010.487855.
573 27. Armenakis, C.; Cyr, I.; Papanikolaou, E. Change detection methods for the revision of topographic
574   databases. *Internatioanl Archives of Photogrammetry Remote Sensing and Spatial Information Sciences* **2002**, *34*,
575   792-797.
576 28. Hussain, M.; Chen, D.; Cheng, A.; Wei, H.; Stanley, D. Change detection from remotely sensed images:
577   From pixel-based to object-based approaches. *ISPRS Journal of Photogrammetry and Remote Sensing* **2013**, *80*,
578   91-106, https://doi.org/10.1016/j.isprsjprs.2013.03.006.
579 29. Zhang, K.; Whitman, D.; Leatherman, S.; Robertson, W. Quantification of Beach Changes Caused by
580   Hurricane Floyd Along Florida's Atlantic Coast Using Airborne Laser Surveys. *Journal of Coastal Research*
581   **2005**, 123-134, https://doi.org/10.2112/02057.1.
582 30. IHO. *S-32: Hydrographic Dictionary - English*; International Hydrographic Bureau: Monaco, 1994;
583   http://hd.iho.int/en/index.php/Main_Page.
584 31. IHO. *S-65: Electronic Navigational Charts (ENCs) "Production, Maintenance and Distribution Guidance"*; Edition
585   2.1.0; International Hydrographic Organization: Monaco, 2017.
586 32. IHO. *S-57: Transfer standard for digital hydrographic data*; Edition 3.1; International Hydrographic
587   Organization: Monaco, 2000.
588 33. Alexander, L. Electronic Charts. In *The American Practical Navigator*, National Imaging and Mapping
589   Agency: Bethesda, MD, USA, 2003; pp 199-215.
590 34. Theobald, D.M. Topology revisited: representing spatial relations. *International Journal of Geographical*
591   *Information Science* **2001**, *15*, 689-705, https://doi.org/10.1080/13658810110074519.
592 35. Hughes Clarke, J.E. The Impact of Acoustic Imaging Geometry on the Fidelity of Seabed Bathymetric
593   Models. *Geosciences* **2018**, *8*, 109.
594 36. De Wulf, A.; Constales, D.; Stal, C.; Nuttens, T. *Accuracy aspects of processing and filtering of multibeam data:*
595   *grid modeling versus TIN based modeling*, FIG Working week, 2012; pp 6-10.
596 37. Delone, B. Sur la sphère vide. A la mémoire de Georges Voronoi. *Bull. Acad. Sci. URSS. Cl. Sci. Math.* **1934**,
597   *6*, 793-800, http://mi.mathnet.ru/eng/izv4937.
598 38. Rebay, S. Efficient Unstructured Mesh Generation by Means of Delaunay Triangulation and Bowyer-
599   Watson   Algorithm.   *Journal   of   Computational   Physics*   **1993**,   *106*,   125-138,
600   https://doi.org/10.1006/jcph.1993.1097.
601 39. Su, P.; Scot Drysdale, R.L. A comparison of sequential Delaunay triangulation algorithms. *Computational*
602   *Geometry* **1997**, *7*, 361-385, https://doi.org/10.1016/S0925-7721(96)00025-9.
603 40. Cheng, S.-W.; Dey, T.K.; Shewchuk, J. Algorithms for constructing Delaunay triangulations. In *Delaunay*
604   *Mesh Generation*, Chapman and Hall/CRC: 2016.
605 41. Barber, C.B.; Dobkin, D.P.; Huhdanpaa, H. The quickhull algorithm for convex hulls. *ACM Trans. Math.*
606   *Softw.* **1996**, *22*, 469-483, https://doi.org/10.1145/235815.235821.
607 42. Vince, J. *Geometry for computer graphics: formulae, examples and proofs*. Springer Science & Business Media:
608   2006; https://doi.org/10.1007/978-1-84628-997-2.
609 43. NOAA. *Hydrographic Surveys Specifications and Deliverables*; Edition April 2018; National Oceanic and
610   Atmospheric Administration, National Ocean Service: 2018; p 159.
611 44. Shimrat, M. Algorithm 112: Position of point relative to polygon. *Commun. ACM* **1962**, *5*, 434,
612   10.1145/368637.368653.
613 45. Haines, E. Point in polygon strategies. In *Graphics gems IV*, Paul, S.H., Ed. Academic Press Professional,
614   Inc.: 1994; pp 24-46.
615 46. Gillies, S.; Bierbaum, A.; Lautaportti, K.; Tonnhofer, O. Shapely: manipulation and analysis of geometric
616   objects. 2007; https://github.com/Toblerity/Shapely.
617 47. van Rossum, G. *The Python Language Reference: Release 3.6.4*. 12th Media Services: 2018; p 168.
618 48. Behnel, S.; Bradshaw, R.; Citro, C.; Dalcin, L.; Seljebotn, D.S.; Smith, K. Cython: The Best of Both Worlds.
619   *Computing in Science and Engg.* **2011**, *13*, 31-39, https://doi.org/10.1109/MCSE.2010.118.
620 49. The Qt Framework. https://www.qt.io/what-is-qt/ (August 2018).
621 50. Hunter, J.D. Matplotlib: A 2D Graphics Environment. *Computing in Science & Engineering* **2007**, *9*, 90-95,
622   https://doi.org/10.1109/MCSE.2007.55.

623   51. Warmerdam, F. The Geospatial Data Abstraction Library. In *Open Source Approaches in Spatial Data*
624   *Handling*, Hall, G.B.; Leahy, M.G., Eds. Springer Berlin Heidelberg: Berlin, Heidelberg, 2008; pp 87-104,
625   https://doi.org/10.1007/978-3-540-74831-1_5.
626   52. IHO. *S-101 Value Added Roadmatp*; Edition April 2016; International Hydrographic Organization: 2016.
627   53. Hughes Clarke, J.E. Multibeam Echosounders. In *Submarine Geomorphology*, Micallef, A.; Krastel, S.; Savini,
628   A., Eds. Springer International Publishing: Cham, 2018; pp 25-41, https://doi.org/10.1007/978-3-319-57852-
629   1_3.
630   54. Lurton, X.; Augustin, J.M. A Measurement Quality Factor for Swath Bathymetry Sounders. *IEEE Journal of*
631   *Oceanic Engineering* **2010**, *35*, 852-862, https://doi.org/10.1109/JOE.2010.2064391.
632   55. Masetti, G.; Kelley, J.G.W.; Johnson, P.; Beaudoin, J. A Ray-Tracing Uncertainty Estimation Tool for Ocean
633   Mapping. *IEEE Access* **2018**, *6*, 2136-2144, https://doi.org/10.1109/ACCESS.2017.2781801.
634   56. IHO. *S-44: Standards for Hydrographic Surveys*; Edition 5; International Hydrographic Organization:
635   Monaco, 2008.
636   57. IHO. *C-13: Manual Of Hydrography*; Edition 1.04; International Hydrographic Organization: Monaco, 2011.
637   58. Kastrisios, C.; Pilikou, M. Nautical cartography competences and their effect to the realisation of a
638   worldwide Electronic Navigational Charts database, the performance of ECDIS and the fulfilment of IMO
639   chart carriage requirements. *Marine Policy* **2017**, *75*, 29-37, https://doi.org/10.1016/j.marpol.2016.10.007.
640   59. Paul Chew, L. Constrained delaunay triangulations. *Algorithmica* **1989**, *4*, 97-108,
641   https://doi.org/10.1007/BF01553881.
642   60. Hjelle, Ø.; Dæhlen, M. Constrained Delaunay Triangulation. In *Triangulations and Applications*, Springer
643   Berlin Heidelberg: Berlin, Heidelberg, 2006; pp 113-129, https://doi.org/10.1007/3-540-33261-8_6.
644   61. Calder, B.R.; Rice, G. Computationally efficient variable resolution depth estimation. *Computers &*
645   *Geosciences* **2017**, *106*, 49-59, https://doi.org/10.1016/j.cageo.2017.05.013.
646   62. IHO. *S-4: Regulations of the IHO for International (INT) Charts and Chart Specifications of the IHO*; Edition 4.6.0;
647   International Hydrographic Organization: Monaco, 2000.
648